

**Dimensional crossover in self-intercalated antiferromagnetic  $V_5S_8$  nanoflakes**

Zhang Zhou<sup>1,\*</sup>, Xiaoxu Zhao<sup>2,\*</sup>, Liangmei Wu,<sup>1</sup> Hongtao Liu,<sup>1</sup> Jiancui Chen<sup>1</sup>, Chuanyin Xi,<sup>3</sup> Zhaosheng Wang,<sup>3</sup> Enke Liu<sup>1</sup>, Wu Zhou,<sup>1,†</sup> Stephen J. Pennycook,<sup>1</sup> Sokrates T. Pantelides<sup>5,1</sup>, Xiao-Guang Zhang<sup>6,†</sup>, Lihong Bao<sup>1,4,†</sup> and Hong-Jun Gao<sup>1,4</sup>

<sup>1</sup>*Institute of Physics & University of Chinese Academy of Sciences, Chinese Academy of Sciences, P. O. Box 603, Beijing 100190, People's Republic of China*

<sup>2</sup>*Department of Materials Science & Engineering, National University of Singapore, Singapore 117575, Singapore*

<sup>3</sup>*High Magnetic Field Laboratory of the Chinese Academy of Sciences, Hefei, Anhui 230031, People's Republic of China*

<sup>4</sup>*Songshan Lake Materials Laboratory, Dongguan, Guangdong 523808, People's Republic of China*

<sup>5</sup>*Department of Physics and Astronomy and Department of Electrical and Computer Engineering, Vanderbilt University, Nashville, Tennessee 37235, USA*

<sup>6</sup>*Department of Physics and the Quantum Theory Project, University of Florida, Gainesville, Florida 32611, USA*



(Received 24 February 2022; accepted 13 June 2022; published 24 June 2022)

Electronic and magnetic ordered states are strongly correlated to the dimensions of matter. Here we report a dimensional crossover in self-intercalated antiferromagnetic  $V_5S_8$  nanoflakes. The transition of three-dimensional (3D) to two-dimensional (2D) transport, evidenced by thickness-independent conductivity, occurs when the thickness of  $V_5S_8$  flakes is reduced to  $\sim 7.3$  nm. At low temperatures, 3D transport follows Fermi liquid behavior, but 2D transport suggests the emergence of Kondo physics with a logarithmic dependence on the temperature and a negative magnetoresistance of a 5.0 nm thick  $V_5S_8$  flake at low temperatures for both in-plane and perpendicular magnetic fields. At temperatures higher than 6 K, the magnetoresistance is positive and parabolically dependent on the magnetic field, indicating suppression of the antiferromagnetic order. Based on a simple magnon gas model, a temperature-independent effective magnon moment ( $\sim 1g\mu_B$ ) is extracted from the Hall coefficient for all  $V_5S_8$  flakes with different thicknesses. Our results reveal that dimensional crossover plays an important role in tuning the electronic properties in 2D metallic transition-metal dichalcogenides (TMDs).

DOI: [10.1103/PhysRevB.105.235433](https://doi.org/10.1103/PhysRevB.105.235433)

**I. INTRODUCTION**

Dimensional crossover [1–4] refers to the change of physical properties of a material as its dimensionality is reduced. When thinning three-dimensional (3D) bulk materials down to their two-dimensional (2D) limit, enhanced thermal and quantum fluctuations can lead to the emergence of exotic properties, examples of which include quantum critical transition in 2D  $CeIn_3$  and enhanced thermal conductivity in graphene [5,6]. Van der Waals-coupled layered materials offer a unique platform for dimensional crossover in which there is a dominant 2D plane, with the interaction along the third dimension already weak. The recent discovery of intrinsic ferromagnetism in few- and monolayer van der Waals crystals such as  $CrI_3$  [7],  $Fe_3GeTe_2$  [8,9], and  $VSe_2$  [10], has ignited broad research interest in the evolution of magnetic order with reduced thickness, interlayer stacking order, and other competing and coexisting ordered electronic states [11].

Monolayer vanadium-based transition-metal dichalcogenides  $VX_2$  ( $X = S, Se, Te$ ) have been theoretically predicted to be intrinsically ferromagnetic [12,13]. Ferromagnetism has indeed been observed in mono- or few-layer  $VSe_2$  [10,14]. When vanadium ions are intercalated into the van der Waals

gap between adjacent  $VX_2$  layers, localized magnetic moments are induced on the intercalated V sites and Kondo-effect features are observed in thick  $VTe_2$  layers [15]. As a self-intercalated compound,  $V_5S_8$  is formed by intercalating 25% excess V atoms into sites in the van der Waals gap between adjacent  $VS_2$  layers, possessing a monoclinic crystal structure [space group  $C2/m$ , Fig. 1(a)]. Only the intercalated V atoms ( $V^1$ ) bear a magnetic moment, while the  $VS_2$  layers provide conducting electrons [16], facilitating an antiferromagnetic (AFM) ordering [17].

The transport behavior has been clarified in the  $s-d$  model, where the conducting charges are scattered from magnons through the  $s-d$  exchange interaction [18,19], or equivalently referred to as the Kondo model [20]. The Kondo lattice behavior in  $V_5S_8$  bulk crystals is revealed by a heavy fermion (HF) state with large Sommerfeld coefficient [21]. A similar Kondo effect has also been observed in  $(Cu_{2/3}V_{1/3})V_2S_4$  [22]. When the thickness of  $V_5S_8$  flakes is reduced, the antiferromagnetic order is suppressed [23] and a weak ferromagnetic order emerges at a thickness of 3.2 nm [24]. However, whether the electron correlation in  $V_5S_8$  crystals is enhanced or suppressed by dimensional crossover still remains unresolved.

Here we report the observation of dimensional crossover in  $V_5S_8$  nanoflakes. Measured thickness-independent conductivity of  $V_5S_8$  flakes shows transition from 3D to 2D below 7.3 nm. By combining analyses of temperature dependence of the conductance and magnetoresistance, we

\*These authors contributed equally to this work.

†wuzhou@ucas.ac.cn; xgz@ufl.edu; lhbao@iphy.ac.cn

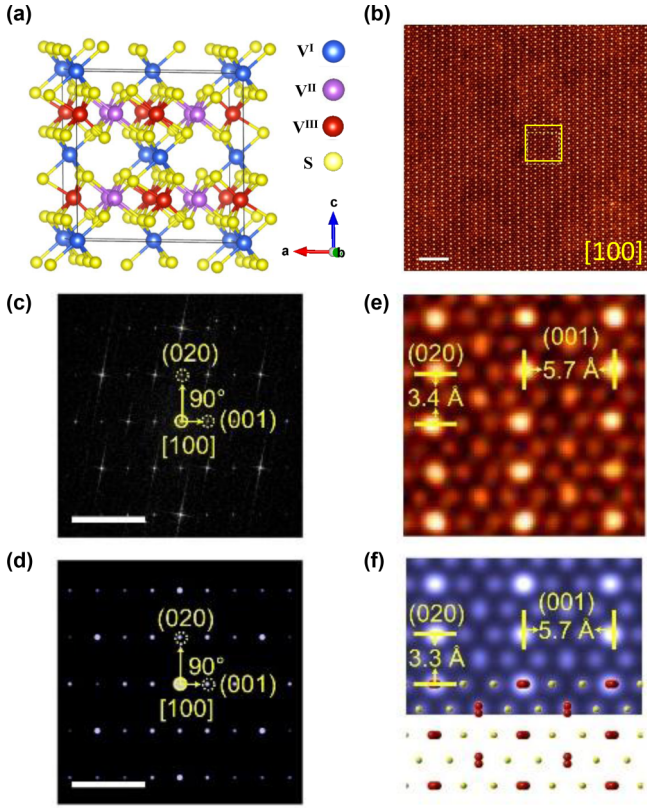


FIG. 1. Structural characterization of  $V_5S_8$  flakes. (a) The atomic structure of  $V_5S_8$ . Different colors are used to distinguish three types of vanadium atoms, labeled  $V^I$ ,  $V^{II}$ , and  $V^{III}$ , respectively. (b) Atomic-resolution STEMADF image viewed along  $[100]$  zone axis, and its (c) corresponding FFT pattern. (d) Simulated SAED pattern basing on the theoretical  $V_5S_8$  atomic model along  $[100]$  zone axis, (e) enlarged image of the yellow box region in (b), and (f) simulated image overlaid with the atomic model along  $[100]$  zone axis. Scale bars: 2 nm in (b),  $5 \text{ nm}^{-1}$  in (c), (d).

show that, below 6 K, 3D transport is characterized by typical Fermi liquid behavior, but 2D transport reveals the emergence of the Kondo effect. Above 6 K, the antiferromagnetic order is suppressed and the positive magnetoresistance is parabolically dependent on the magnetic field. Fitting the anomalous Hall coefficient to a simple magnon gas model, a temperature-independent effective magnon moment of  $\sim 1g\mu_B$  is extracted at temperatures above the Néel temperature. Our results highlight the role of dimensional crossover in tuning the electronic properties, phase evolution, and electron correlations in 2D metallic TMDs.

## II. EXPERIMENTAL METHODS

Ultrathin  $V_5S_8$  flakes were synthesized via the chemical vapor deposition (CVD) method inside a furnace with a 1 in. diameter quartz tube [23,24]. Solid  $VCl_3$  and sulfur with evaporation temperature of  $300^\circ\text{C}$  and  $150^\circ\text{C}$ , respectively, in a mixed  $\text{Ar}/\text{H}_2$  (95/5 sccm) carrier gas, were used as precursors. By varying the location of a  $\text{SiO}_2/\text{Si}$  substrate downstream from the  $VCl_3$  precursor, the deposition temperature can be tuned from  $550^\circ\text{C}$  to  $600^\circ\text{C}$  and  $V_5S_8$  flakes

with thickness ranging from 5.5 nm to tens of nanometers and lateral size up to  $\sim 20 \mu\text{m}$  can be obtained. The thickness of the  $V_5S_8$  flakes was determined with an atomic force microscope using the tapping mode (Dimension Edge, Bruker). Atomic-resolution scanning transmission electron microscopy (STEM)–annular dark field (ADF) images were taken using a JEOL ARM200F STEM equipped with an ASCOR aberration corrector operating at 60 kV. The collection angle was  $30\text{--}110 \text{ mrad}$  in order to enhance the S contrast. The as-grown  $V_5S_8$  nanosheets were transferred to a precleaned  $\text{SiO}_2/\text{Si}$  substrate by a direct face to face method [25]. Hall-bar devices were fabricated by a standard electron-beam lithography technique, followed by electron-beam evaporation of Ti/Au (5/60 nm) electrodes. Considering the possible anisotropy of conductivity along different axes, the metal contacts were carefully aligned vertically to the edge when deriving 2D and 3D conductivity. Transport measurements were performed in a Physical Property Measurement System (PPMS, Quantum Design Inc.) cryostat. A constant  $1 \mu\text{A}$  ac current above 10 Hz was applied for all the magnetotransport measurements. Transport measurements at high field were done at the High Magnetic Field Laboratory of the Chinese Academy of Sciences, Hefei. The temperature-dependent Hall coefficient ( $R_H$ ) was obtained at fixed magnetic field, with the temperature warming slowly enough ( $0.6 \text{ K/min}$ ) to ensure accurate temperature measurement. A symmetrized (antisymmetrized) procedure was performed to remove the  $R_{xx}$  component in the  $R_{xy}$  data and the  $R_{xy}$  component in the  $R_{xx}$  data:

$$R_{xy}^{\text{sym}} = [R_{xy}(\mu_0 H) - R_{xy}(-\mu_0 H)]/2,$$

$$R_{xx}^{\text{sym}} = [R_{xx}(\mu_0 H) + R_{xx}(-\mu_0 H)]/2,$$

$$MR = [R_{xx}^{\text{sym}}(\mu_0 H) - R_{xx}(0)]/R_{xx}(0) \times 100\%.$$

## III. RESULTS AND DISCUSSION

### A. Characterization of $V_5S_8$ flakes

A typical optical image of  $V_5S_8$  flakes on the  $\text{SiO}_2/\text{Si}$  substrate is shown in Fig. S1(a) in the Supplemental Material [26]. The crystallographic unit cell of  $V_5S_8$  is schematically shown in Fig. 1(a). Scanning transmission electron microscopy–annular dark field (STEMADF) imaging and image simulation were employed to unveil the crystal structure of the  $V_5S_8$  flakes. Electron energy loss spectroscopy (EELS) (Fig. S1(b) [26]) first confirmed that the as-grown flakes are composed of vanadium and sulfur elements only. The atomic-resolution STEMADF image [Fig. 1(b)] shows that the as-grown vanadium sulfide flake is homogeneous without any defects. The single set of spots showing in the fast Fourier transform (FFT) pattern [Fig. 1(c)] and selected area electron diffraction (SAED) pattern (Fig. S1 [26]) matches well the monoclinic structure of  $V_5S_8$  (space group  $C2/m$ ,  $a = 11.356 \text{ \AA}$ ,  $b = 6.648 \text{ \AA}$ ,  $c = 11.298 \text{ \AA}$ ,  $\beta = 90.60^\circ$ ) along the  $[100]$  zone axes [23,24,27,28]. The atomically resolved image shown in Fig. 1(e) clearly shows well-defined lattice spacings of 3.4 and 5.7  $\text{\AA}$ , which are consistent with the theoretical values [Fig. 1(f)] of the interplanar distances of 3.3  $\text{\AA}$  for (020) planes and 5.7  $\text{\AA}$  for (001) planes in an ideal  $V_5S_8$  crystal along the  $[100]$  zone axis [27,28], as highlighted in the simulated image [Fig. 1(f)]. In order to further validate that the

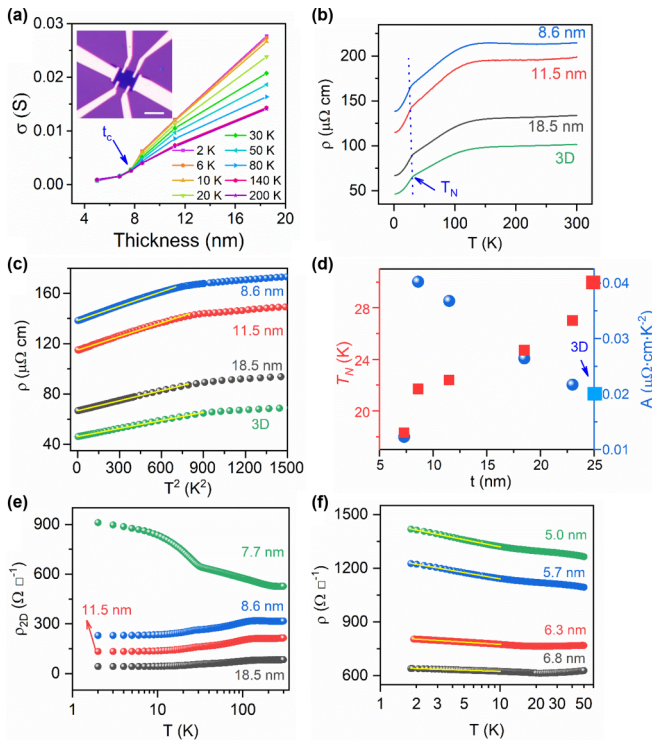


FIG. 2. Dimensional crossover in  $V_5S_8$  thin flakes. (a) Thickness-dependent conductivity of  $V_5S_8$  flakes at different temperatures. The arrow indicates the critical thickness ( $t_c$ ). The inset shows an optical-microscope image of a typical Hall-bar device on a  $V_5S_8$  flake. The scale bar is  $10 \mu\text{m}$ . (b) Temperature-dependent resistivity for the thicker flakes. The 3D resistivity is extracted from linear fitting of conductivity as a function of thickness at above critical thickness in (b). (c) The Fermi liquid-like behavior ( $\rho \propto T^2$ ) below 30 K in the thicker ( $\geq 8.6$  nm) flakes. The horizontal axis is plotted as  $T^2$ . The solid lines are fitting curves. (d) The  $T^2$ -term coefficient ( $A$ ) and Néel temperature ( $T_N$ ) derived from  $V_5S_8$  flakes with various thicknesses. (e) Temperature-dependent 2D resistivity of thick  $V_5S_8$  flakes by subtracting the contributions from 3D bulk. (f) Temperature-dependent resistivity of thin  $V_5S_8$  flakes. At low temperatures, linearly fitted curves (yellow lines) show a universal negatively logarithmic dependence of resistivity on the temperatures, revealing the presence of Kondo behavior.

as-grown flakes are  $V_5S_8$  flakes, the same analysis was carried out when the flake was tilted to the  $[210]$  plane, as shown in Figs. S1(c)–S1(g) [26]. Therefore, it can be concluded that the as-grown vanadium sulfide flakes are  $V_5S_8$  crystals.

### B. Dimensional crossover in ultrathin $V_5S_8$ flakes

A typical Hall-bar device on a  $V_5S_8$  flake is shown in the inset of Fig. 2(a). For thick  $V_5S_8$  flakes ( $\geq 7.7$  nm) the temperature-dependent resistivity exhibits bulk behavior [21,27]. As the flake gets thinner to  $\sim 7.3$  nm and below, an upturn of resistivity emerges and the normalized resistivity  $R(2 \text{ K})/R(300 \text{ K})$  increases monotonically with temperature, as shown in Fig. S2(a) [26]. The conductivity scales linearly with the thickness at different temperatures for  $V_5S_8$  flakes thicker than 7.7 nm, which is a hallmark of 3D conductivity, as shown in Fig. 2(a). For thinner  $V_5S_8$  flakes, the conductivity does not show evident changes with thickness, indicating a

2D transport behavior. In this regard, the conductivity of  $V_5S_8$  flakes can be described as two independent parallel channels containing the 2D and 3D contributions, respectively:

$$\sigma = \sigma_{2D} + \sigma_{3D}(t - t_c), \quad t > t_c, \quad (1)$$

where  $t$  is the total thickness,  $t_c$  is the critical thickness,  $\sigma_{2D}$  is the 2D conductivity, and  $\sigma_{3D}$  is the 3D conductivity.

The 3D conductivity is extracted from the slope of the conductivity-thickness curves by linear fitting and the converted 3D resistivity is plotted in Fig. 2(b). The extracted 3D resistivity reproduces well the temperature-dependent behavior of bulk single crystals with a residual resistance ratio [RRR =  $R(300 \text{ K})/R(2 \text{ K})$ ] of 2.5, similar to that reported in bulk crystals [21,27]. A remarkable decrease of resistivity is observed in the AFM state with a kink at the Néel temperature ( $T_N$ ), which is extracted from the peak of the  $d\rho/dT$  (shown in Figs. S2(b)–2(j) [26]).  $T_N$  decreases as the flakes get thinner, summarized in Fig. 2(d). For flakes thinner than 7.3 nm, the local maximum disappears, indicating the breakdown of AFM order. The critical thickness  $t_{2D}$  is derived to be  $\sim 7$  nm at the emergence of resistivity upturn (see Fig. S2(a) [26]), which is also confirmed by the deviation from linear behavior in conductivity-thickness curves, as shown in Fig. 2(a). For thick  $V_5S_8$  flakes ( $> 7.3$  nm), the resistivity below  $T_N$  matches the Fermi liquid behavior ( $\rho = \rho_0 + AT^2$ ) very well, as shown in Fig. 2(d). The extracted coefficient ( $A$ ) shows an increasing trend with reduced thickness [Fig. 2(d)], suggesting enhanced electron correlations with reduced thickness [5]. However, when reduced close to the critical thickness, the Fermi liquid coefficient ( $A$ ) drops down suddenly, indicating the emergence of dimensional crossover.

The 2D contribution ( $\rho_{2D}$ ) is obtained by subtracting the 3D conductivity from the total conductivity and is plotted in Fig. 2(e), showing a logarithmic temperature dependence. For  $V_5S_8$  flakes thicker than 7.7 nm, the 2D resistivity at low temperatures remains almost constant. For flakes thinner than the critical thickness, the resistivity scales with the logarithm of the temperature below 10 K, suggesting a possible Kondo lattice-like behavior emerges. This dimensional crossover is revealed with a parallel conductivity model with independent 3D and 2D transport channels. Similar behavior has also been observed in Kondo systems via substitutional effects of isoelectric magnetic and nonmagnetic atoms, such as the  $\text{Ce}(\text{Pt}_{1-x}\text{Ni}_x)\text{Sn}$  and  $(\text{Ce}_{1-x}\text{La}_x)_3\text{Bi}_4\text{Pt}_3$  alloys [29]. However, the 2D regime typically comes at much thinner flake of less than  $\sim 3.0$  nm for  $\text{VSe}_2$  [25] and  $\text{Fe}_3\text{GeTe}_2$  [8]. As is known, the upturn in resistivity at low temperatures could also be attributed to weak localization or impurity Kondo effect [30,31]. To uncover the origin of the resistivity upturn, magnetotransport measurements are performed.

### C. Magnetoresistance of $V_5S_8$ nanoflakes

Figure 3 shows the temperature-dependent resistivity of  $V_5S_8$  thin flakes at various magnetic fields. For the 11.5 nm flake, the kink at  $T_N$  is gradually suppressed with increasing magnetic fields, while the Fermi liquid behavior remains [Fig. 3(a)]. As shown in Fig. 3(d), the extracted  $T^2$ -term coefficient ( $A$ ) (Supplemental Figs. S3(a)–S3(d) [26]) shows a slight decrease with the increase of magnetic field, suggesting

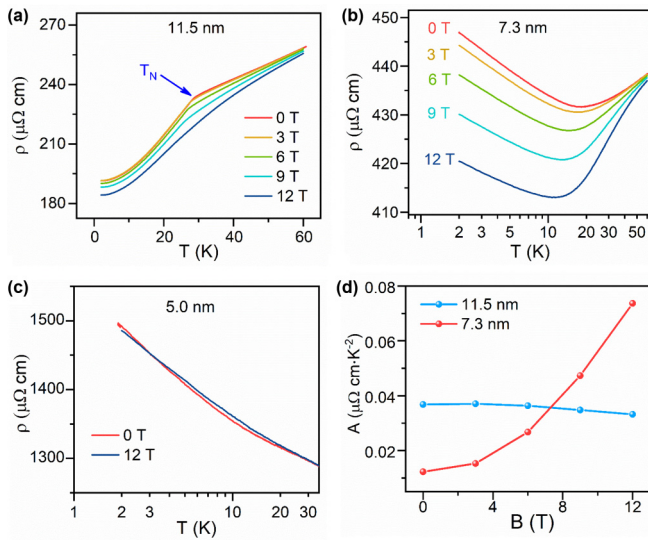


FIG. 3. Temperature-dependent resistivity of  $V_5S_8$  flakes with thickness of (a) 11.5 nm, (b) 7.3 nm, and (c) 5.0 nm at various magnetic fields, respectively. (d) The Fermi liquid coefficient  $A$  derived from fitting.

a field-induced metamagnetic state [23]. For the 7.3 nm flake, the upturn in resistivity below  $\sim 10$  K gets suppressed with increasing magnetic field but remains with almost the same slope at magnetic fields up to 12 T, indicating that the resistivity upturn is neither coming from a weak-localization effect nor from an impurity Kondo effect. The coefficient  $A$  extracted in the temperature range below  $T_N$  (Supplemental Figs. S3(e)–S3(i) [26]) increases with increasing magnetic field, suggesting enhanced electron-electron correlations. In the 5.0 nm flake, the resistivity changes little with magnetic fields and the negatively logarithmic dependence on temperatures below 10 K remains, indicating that after the dimensional crossover in the  $V_5S_8$  flakes, the electron-electron interaction is robust upon applying the magnetic field.

With decreasing thickness in  $V_5S_8$  flakes, the spin-flopping (SF) transition becomes weaker, and the positive MR before the SF transition disappears, indicating the suppression of AFM order in thinner flakes, as shown in Figs. 4(a) and 4(b). An evident SF transition from antiferromagnetic to paramagnetic phase in field-dependent MR at around 4 T is observed, as in bulk crystals [32]. With increasing magnetic fields, MR is firstly positive in the AFM state, and then changes to negative after the SF transition [32]. Above  $T_N$ , MR is still negative to rather high temperatures. The negative MR indicates the inelastic scattering of conduction charges by local moments [19]. However, the MR in the 5.0 nm thick flake shows negative to positive transition at 4 K, similar to that reported in a 3-ML (monolayer)  $V_5Se_8$  grown by MBE [33]. Below 4 K, MR is negative at low fields but starts showing a positive trend at higher fields. Above 4 K the MR is positive for all fields. This suggests the negative MR at low fields is correlated with the  $-\ln T$  behavior in resistivity. Notably when the flake is aligned parallel to the field, the MR behaves very similarly to that perpendicular to the field, as shown in Fig. 4(d), with the same trend and magnitude. It is also expected in the case of a Kondo effect with an isotropic

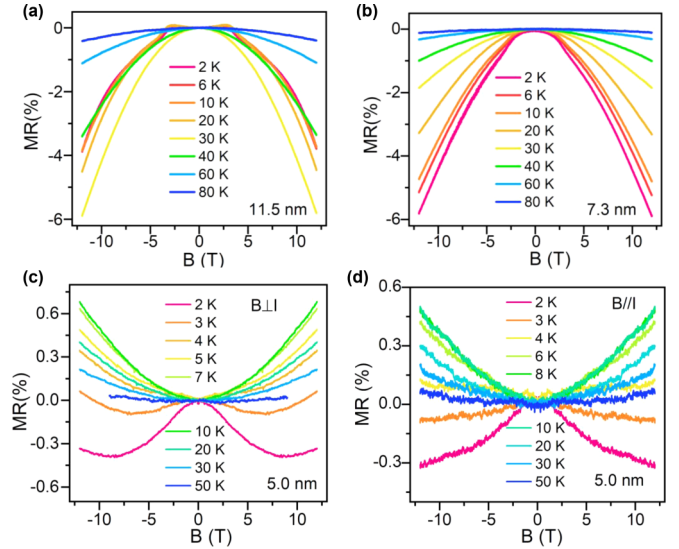


FIG. 4. Magnetoresistivity in  $V_5S_8$  thin flakes with different thicknesses at various temperatures. (a) 11.5 nm, (b) 7.3 nm, and (c), (d) 5.0 nm. The magnetic field is perpendicular to the flake plane in (a)–(c), and is aligned parallel to the current direction in the flake plane in (d).

$s$ - $d$  exchange interaction, ruling out the possibility of weak localization for which the phase interference is sensitive to field orientation [30]. Signatures of the Kondo effect have also been observed in bulk  $VSe_2$  crystals [34] and  $VTe_2$  nanoplates [15], which is believed to be due to a slight amount of intercalated paramagnetic V atoms. In the case of  $V_5S_8$ , it is a naturally self-intercalated system and Kondo lattice behavior has been found in the bulk crystals [21]. A large magnetic field is required to observe the MR transition in Kondo systems since Kondo coupling is remarkably robust upon increasing magnetic fields [35–37]. Nakanishi *et al.* reported the nearly linear magnetization behavior with the saturation field of 27 T in  $V_5S_8$  crystals [38]. The transport properties of  $V_5S_8$  thin flakes up to 38 T are shown in Fig. S4 [26]. The MR changes from negative to positive at 27 T. With the thickness reduced to 7.3 nm, MR is all negative at high fields.

#### D. Anomalous Hall coefficient of $V_5S_8$ nanoflakes

The anomalous Hall effect (AHE) is not supposed to appear in collinear antiferromagnetic systems without intrinsic magnetization [39]. Below  $T_N$ , the transition in Hall resistivity ( $\rho_H$ ) at low fields suggests the SF transition, as shown in Fig. S4(b) [26]. This is due to the suppression of AFM order with reduced thickness [23,24]. The temperature-dependent Hall coefficient at certain external magnetic field is shown in Figs. 5(a)–5(c) with three  $V_5S_8$  flakes of thicknesses of 11.5 nm [Fig. 5(a)], 7.3 nm [Fig. 5(b)], and 5.0 nm [Fig. 5(c)], respectively. In the AFM state before the spin-flopping at relatively small fields and temperatures below the Néel temperature, remarkable deviation from that of the paramagnetic state is observed in the Hall coefficient. Above the Néel temperature, the temperature-dependent Hall coefficient stays the same at different magnetic fields. The onset of sudden change in the Hall coefficient is marked as the coherent Kondo

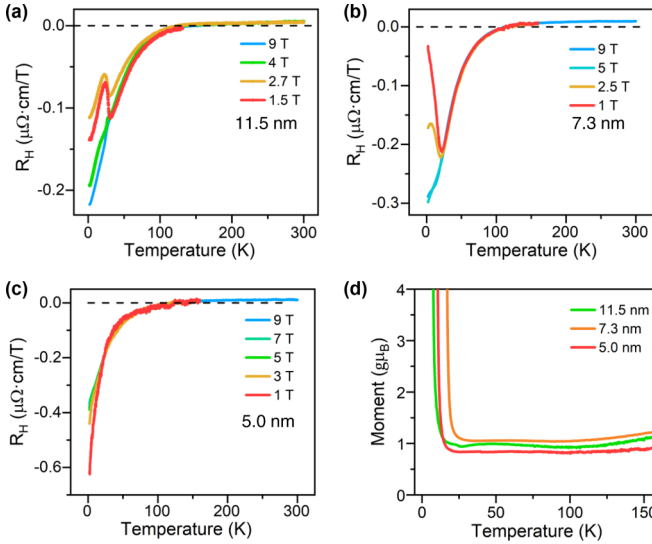


FIG. 5. Temperature-dependent Hall coefficient ( $R_H$ ) at different external magnetic fields of  $V_5S_8$  flakes with thicknesses of 11.5 nm (a), 7.3 nm (b), and 5.0 nm (c), respectively. (d) The extracted effective magnetic moment of a single magnon at external field of 9 T based on a magnon gas model.

temperature ( $T^*$ ) [40]. Notably the sign reversal of the Hall coefficient is found, with the transition temperature about 136 K for the 11.5 nm flake, 116 K for the 7.0 nm flake, and 119 K for the 5.0 nm flake, respectively, which decreases with reduced thickness compared to that of bulk crystal (150 K) [27].

In AHE the Hall resistance  $R_{xy}$  contains the intrinsic magnetization part except the ordinary part.

$$R_{xy} = R_O B + R_A \mu_0 M. \quad (2)$$

In  $V_5S_8$  bulk crystals the Hall coefficient  $R_H$  has been found to be linearly dependent on the magnetic susceptibility  $\chi$  [21] and the change of the Hall coefficient is mainly attributed to the intrinsic magnetization. The magnetic moment could be extracted by fitting the temperature-dependent magnetic susceptibility. The magnetization behavior of a  $V_5S_8$  bulk crystal follows the Curie-Weiss Law above 140 K while it deviates from it in the incoherent Kondo regime at low temperatures [21,41]. In a noninteracting magnon gas model, the total magnetization can be described by the Langevin function:

$$M = \coth(\alpha) - \frac{1}{\alpha}, \quad (3)$$

$$\alpha = \frac{mB_{\text{total}}}{k_B T}, \quad (4)$$

where  $m$  is the moment of a single magnon, the total magnetic field is  $B + \lambda M$  under the mean-field approximation, and  $\lambda$

is the coupling coefficient. Equation (3) is a self-consistent equation for  $M$ . Once  $M$  is solved,  $R_{xy}$  can then be written as a function of the external field ( $B$ ) and temperature ( $T$ ). To simplify the solution, we expand the right-hand side of Eq. (3) to linear order in  $M$  to allow an analytic solution. The Hall coefficient as a function of temperature ( $T$ ) and external fields ( $B$ ) is found to be

$$R_H = R_0 + R_A \left[ \coth(\alpha_0) - \frac{1}{\alpha_0} \right] / \left[ 1 + \frac{\lambda R_A m}{B} \left( \frac{\alpha_0}{\sinh^2(\alpha_0)} - \frac{1}{\alpha_0} \right) \right], \quad (5)$$

where  $\alpha_0 = mB/k_B T$ . The coefficients  $R_0$ ,  $R_A$ ,  $m$ , and  $\lambda$  are fitted to the temperature-dependent  $R_H$  curve at 9 T (Supplemental Table S1 [26]). The effective magnetic moment  $m$  is fitted for each temperature, yielding  $\sim 1 g\mu_B$  per magnon ( $g$  is the Landé  $g$  factor and  $\mu_B$  is the Bohr magneton). The extracted effective moment stays nearly constant at temperatures higher than the Néel temperature, and diverges in the AFM state below the Néel temperature, as shown in Fig. 5(d). In turn, the nearly constant magnon moment over the temperature range above the Néel temperature and for samples of different thicknesses confirms our model.

#### IV. SUMMARY

We have obtained ultrathin  $V_5S_8$  flakes with atomic-resolution STM imaging to reveal the intercalated structure. From the transport studies of various thicknesses, a 3D to 2D dimensional crossover is found in the temperature-dependent conductivity with a critical thickness of  $\sim 7$  nm. With reducing thickness, the AFM order is weakened with the decrease of Néel temperature. When further reducing to 5.0 nm, the Kondo effect is revealed with evidence in  $-\ln(T)$  behavior in resistivity and angular-insensitive MR with field. Moreover, based on a simple magnon gas model, the magnon moment is determined from the Hall coefficient. Our results demonstrate that with reduced dimensions, electron-electron correlations can be effectively enhanced in a self-intercalated system. This feature provides another degree of freedom for tuning the electronically ordered state and phase transition in condensed matter.

#### ACKNOWLEDGMENTS

This work was supported by the National Key Research & Development Projects of China (Grants No. 2016YFA0202300 and No. 2018FYA0305800), National Natural Science Foundation of China (Grant No. 61888102), Strategic Priority Research Program of Chinese Academy of Sciences (CAS, Grants No. XDB30000000 and No. XDB28000000), Youth Innovation Promotion Association of CAS (Grant No. Y201902), and CAS Project for Young Scientists in Basic Research (Grant No. YSBR-003).

- [1] W. Li, S. Ponce, and F. Giustino, *Nano Lett.* **19**, 1774 (2019).  
 [2] A. Pasztor, A. Scarfato, C. Barreateau, E. Giannini, and C. Renner, *2D Mater.* **4**, 041005 (2017).

- [3] C. Liu, Y. Zang, W. Ruan, Y. Gong, K. He, X. Ma, Q.-K. Xue, and Y. Wang, *Phys. Rev. Lett.* **119**, 176809 (2017).  
 [4] M. P. McDonald, R. Chatterjee, J. Si, B. Janko, and M. Kuno, *Nat. Commun.* **7**, 12726 (2016).

- [5] H. Shishido, T. Shibauchi, K. Yasu, T. Kato, H. Kontani, T. Terashima, and Y. Matsuda, *Science* **327**, 980 (2010).
- [6] S. Ghosh, W. Bao, D. L. Nika, S. Subrina, E. P. Pokatilov, C. N. Lau, and A. A. Balandin, *Nat. Mater.* **9**, 555 (2010).
- [7] B. Huang, G. Clark, E. Navarro-Moratalla, D. R. Klein, R. Cheng, K. L. Seyler, D. Zhong, E. Schmidgall, M. A. McGuire, D. H. Cobden *et al.*, *Nature (London)* **546**, 270 (2017).
- [8] Y. Deng, Y. Yu, Y. Song, J. Zhang, N. Z. Wang, Z. Sun, Y. Yi, Y. Z. Wu, S. Wu, J. Zhu *et al.*, *Nature (London)* **563**, 94 (2018).
- [9] Z. Fei, B. Huang, P. Malinowski, W. Wang, T. Song, J. Sanchez, W. Yao, D. Xiao, X. Zhu, A. F. May *et al.*, *Nat. Mater.* **17**, 778 (2018).
- [10] M. Bonilla, S. Kolekar, Y. Ma, H. C. Diaz, V. Kalappattil, R. Das, T. Eggers, H. R. Gutierrez, M.-H. Phan, and M. Batzill, *Nat. Nanotechnol.* **13**, 289 (2018).
- [11] K. S. Burch, D. Mandrus, and J.-G. Park, *Nature (London)* **563**, 47 (2018).
- [12] Y. Ma, Y. Dai, M. Guo, C. Niu, Y. Zhu, and B. Huang, *ACS Nano* **6**, 1695 (2012).
- [13] H.-R. Fuh, B. Yan, S.-C. Wu, C. Felser, and C.-R. Chang, *New J. Phys.* **18**, 113038 (2016).
- [14] P. Mangelis, P. Vaqueiro, J.-C. Jumas, I. da Silva, R. I. Smith, and A. V. Powell, *J. Solid State Chem.* **251**, 204 (2017).
- [15] H. Liu, Y. Xue, J.-A. Shi, R. A. Guzman, P. Zhang, Z. Zhou, Y. He, C. Bian, L. Wu, R. Ma *et al.*, *Nano Lett.* **19**, 8572 (2019).
- [16] S. Funahashi, H. Nozaki, and I. Kawada, *J. Phys. Chem. Solids* **42**, 1009 (1981).
- [17] I. Kawada, M. Nakano-Onoda, M. Ishii, M. Saeki, and M. Nakahira, *J. Solid State Chem.* **15**, 246 (1975).
- [18] K. Ueda, *J. Phys. Soc. Jpn.* **43**, 1497 (1977).
- [19] K. Usami, *J. Phys. Soc. Jpn.* **45**, 466 (1978).
- [20] O. Zachar and I. Zaliznyak, *Phys. Rev. Lett.* **91**, 036401 (2003).
- [21] J. Niu, W. Zhang, Z. Li, S. Yang, D. Yan, S. Chen, Z. Zhang, Y. Zhang, X. Ren, P. Gao *et al.*, *Chin. Phys. B* **29**, 097104 (2020).
- [22] S. Tewari, *Phys. Rev. B* **69**, 014512 (2004).
- [23] W. J. Hardy, J. Yuan, H. Guo, P. Zhou, J. Lou, and D. Natelson, *ACS Nano* **10**, 5941 (2016).
- [24] J. Niu, B. Yan, Q. Ji, Z. Liu, M. Li, P. Gao, Y. Zhang, D. Yu, and X. Wu, *Phys. Rev. B* **96**, 075402 (2017).
- [25] H. Liu, L. Bao, Z. Zhou, B. Che, R. Zhang, C. Bian, R. Ma, L. Wu, H. Yang, J. Li *et al.*, *Nano Lett.* **19**, 4551 (2019).
- [26] See Supplemental Material at <http://link.aps.org/supplemental/10.1103/PhysRevB.105.235433> for additional STEM images and transport data on V5S8 flakes.
- [27] H. Nozaki, Y. Ishizawa, M. Saeki, and M. Nakahira, *Phys. Lett. A* **54**, 29 (1975).
- [28] M. Knecht, H. Ebert, and W. Bensch, *J. Phys.: Condens. Matter* **10**, 9455 (1998).
- [29] D. T. Adroja, B. D. Rainford, A. J. Neville, and A. G. M. Jansen, *Physica B* **223–224**, 275 (1996).
- [30] G. Bergmann, *Phys. Rep.* **107**, 1 (1984).
- [31] P. A. Lee and T. V. Ramakrishnan, *Rev. Mod. Phys.* **57**, 287 (1985).
- [32] H. Nozaki and Y. Ishizawa, *Phys. Lett. A* **63**, 131 (1977).
- [33] M. Nakano, Y. Wang, S. Yoshida, H. Matsuoka, Y. Majima, K. Ikeda, Y. Hirata, Y. Takeda, H. Wadati, Y. Kohama *et al.*, *Nano Lett.* **19**, 8806 (2019).
- [34] S. Barua, M. C. Hatnean, M. R. Lees, and G. Balakrishnan, *Sci. Rep.* **7**, 10964 (2017).
- [35] M. Jaime, R. Movshovich, G. R. Stewart, W. P. Beyermann, M. G. Berisso, M. F. Hundley, P. C. Canfield, and J. L. Sarrao, *Nature (London)* **405**, 160 (2000).
- [36] H. Xia, Y. Li, M. Cai, L. Qin, N. Zou, L. Peng, W. Duan, Y. Xu, W. Zhang, and Y.-S. Fu, *ACS Nano* **13**, 9647 (2019).
- [37] Z. Wang, T. Zhou, T. Jiang, H. Sun, Y. Zang, Y. Gong, J. Zhang, M. Tong, X. Xie, Q. Liu *et al.*, *Nano Lett.* **19**, 4627 (2019).
- [38] M. Nakanishi, K. Yoshimura, K. Kosuge, T. Goto, T. Fujii, and J. Takada, *J. Magn. Magn. Mater.* **221**, 301 (2000).
- [39] N. Nagaosa, J. Sinova, S. Onoda, A. H. MacDonald, and N. P. Ong, *Rev. Mod. Phys.* **82**, 1539 (2010).
- [40] Y.-f. Yang, *Phys. Rev. B* **87**, 045102 (2013).
- [41] A. B. De Vries and C. Haas, *J. Phys. Chem. Solids* **34**, 651 (1973).